



ELSEVIER

Inorganica Chimica Acta 339 (2002) 89–103

**Inorganica
Chimica Acta**

www.elsevier.com/locate/ica

Synthesis, electrochemical studies, density functional analysis and X-ray structures of *trans,cis,cis*-[RuCl₂(*N*-methylimidazole)₂(SbPh₃)₂] and *trans,cis,cis*-[RuCl₂(4-methylpyrimidine)₂(SbPh₃)₂]. The role of C–H···N and C–H···Cl interactions in pyrimidine pairings and in tuning the angular approach of imidazole residues to metals

Renzo Cini^{a,*}, Cinzia Bellucci^a, Gabriella Tamasi^a, Maddalena Corsini^b,
Marco Fontani^b, Piero Zanello^b

^a Department of Chemical and Biosystem Sciences and Technologies, University of Siena, Via Aldo Moro, I-53100 Siena, Italy

^b Department of Chemistry, University of Siena, Via Aldo Moro, I-53100 Siena, Italy

Received 18 October 2001; accepted 18 January 2002

This study is dedicated to Professor Dr. Helmut Sigel, University of Basel, on the occasion of his 65th birthday

Abstract

The reaction of *trans*-[RuCl₂(SbPh₃)₄] (**1**) (Ph = C₆H₅) (Inorg. Chim. Acta 208 (1993) 189) with tenfold excess *N*-methylimidazole (Meim) and 4-methylpyrimidine (Mepym) in chloroform at reflux under ultrapure nitrogen produced *trans,cis,cis*-[RuCl₂(Meim)₂(SbPh₃)₂] (**2**), and *trans,cis,cis*-[RuCl₂(Mepym)₂(SbPh₃)₂] (**3**), respectively. The compounds were purified and crystallized from ethylacetate and absolute ethanol and gave single crystals of **2**·CH₃COOCH₂CH₃ and **3**, respectively. The X-ray diffraction analyses showed that for both **2** and **3** the ligand substitutions on **1**, takes place in *cis*-positions. The relative orientation of the two Meim and Mepym ligands around the Ru–N vectors is *head-to-head* and *head-to-tail* for **2** and **3**, respectively, in the solid state, whereas free rotation was detected in solution (CDCl₃) at 25 °C. The Ru–N bond distances average 2.108(4) Å, **2**, and 2.131(5) Å, **3**, and are elongated by the *trans* influence and by the steric hindrance from the two SbPh₃ ligands. Intramolecular attractive stacking interactions between one of the phenyl rings and one of the Meim or Mepym ligands in **2** and **3**, attenuate the repulsive steric hindrance within the coordination sphere. The Ru–N–C bond angles for **2** differ by 5.2° but have the opposite trend for the two Meim ligands. This fact agrees with a small energy barrier for the in plane swinging of the Meim ring with respect to the Ru–N line and is related to the C–H···Cl intramolecular interactions. Both the Mepym ligands of **3** have intermolecular interactions of the type C–H···N (N···C, 3.63(1) Å), the two “paired bases” not being coplanar (dihedral angle, 46.5(3)°). A density functional and ab initio optimization analysis at the Becke3LYP/6-31G** level and CCSD(T)/6-31G** level, carried out on the Pym molecule and on the Pym···Pym adduct, confirmed the feasibility of the C–H···N interaction at least for an environment that is not aqueous and allowed computation of a pairing energy of –11.657 and –13.887 kJ mol^{–1}, respectively. Structure optimization analyses were also performed on the model molecules, *trans*-[RuCl₂(SbH₃)₄] at the Becke3LYP/LANL2DZ (6-31G**, Cl, H) level, and *head-to-head* and *head-to-tail trans,cis,cis*-[RuCl₂(Im)₂(SbH₃)₂], *head-to-head* and *head-to-tail trans,trans,trans*-[RuCl₂(Im)₂(SbH₃)₂], *head-to-tail trans,cis,cis* and *trans,trans,trans*-[RuCl₂(Im)₂(PH₃)₂] at the Becke3LYP/LANL2DZ level. The difference between the electronic energies relevant to the two couples of isomers *head-to-head* and *head-to-tail trans,cis,cis*-[RuCl₂(Im)₂(SbH₃)₂] and *trans,trans,trans*-[RuCl₂(Im)₂(SbH₃)₂] is no larger than 2.7 kJ mol^{–1}, showing that inter- and intramolecular weak forces play a significant role in discriminating the most stable isomer, at the solid state. A planar model molecule of the type [Ru(Im)]²⁺ was fully optimized at the Becke3LYP/LANL2DZ level. The computed Ru–N(1)–C(2) bond angle is 126.3° and the computed energy required to bend the angle in plane in the range 118.0–134.0° is less than 5.0 kJ mol^{–1}. This confirms that weak interactions like C–H···Cl can reasonably cause significant changes at the level of the Ru–N–C bending in plane for metal–imidazole complexes. In dichloromethane solution complex **2** displays a chemically reversible Ru(II)/Ru(III)

* Corresponding author. Tel.: +39-0577-234 368; fax: +39-0577-234 177

E-mail address: cini@unisi.it (R. Cini).

oxidation with formal electrode potentials of -0.27 V (versus the ferrocene/ferricinium couple), whereas **3**, *trans,trans,trans*-[RuCl₂(Mepym)₂(PPh₃)₂] (**5**) and *trans,trans,trans*-[RuCl₂(Thz)₂(PPh₃)₂] (**6**) (Thz, 1,3-thiazole) undergo the same type of oxidation process with electrode potential values $+0.08$, $+0.07$ and -0.06 V, respectively. Therefore, **2** looks like the more suitable for protein binding (after oxidation to the mono-cation), when compared to **3**, **5**, and **6**, a step believed to be important for decreasing the toxicity of ruthenium based anticancer drugs.

© 2002 Elsevier Science B.V. All rights reserved.

Keywords: Ruthenium complexes; Imidazole; Pyrimidine; X-ray diffraction; Density functional; Electrochemistry

1. Introduction

Metal complexes containing imidazole and pyrimidine moieties as ligands play a variety of roles in biological systems (see for instance Refs. [1a–1e] and references cited therein). In particular, several complexes of ruthenium(II,III) have become a matter of increasing interest from a bioinorganic perspectives as well as for their electrochemical and catalytical properties [1e–1k,2,3]. A large part of the attention comes because the complexes can act as probes in structural studies for the nucleic acids, because many ruthenium complexes are very promising as antitumor drugs and some of them are under intensive preclinical studies [1e,2,4]. The formation of *cis*-coordinated metal complexes is often a leading step in the cytostatic processes by metal based drugs (see Ref. [1f] and references therein). Furthermore, the antitumoral activity of ruthenium complexes is in general modulated by several redox processes, mostly relevant to the couple Ru(III)/Ru(II) [1k]. In fact, tumor cells have reductive environments with respect to normal tissues, thus favoring Ru(II) species (over the corresponding Ru(III) ones, which have higher affinity for carrier systems, e.g. transferrin). The Ru(II) derivatives mostly link nuclear targets (nucleic acid bases) to exert anti-proliferative activity.

The synthesis and the structural characterization of metal complexes relevant to bioinorganic chemistry was the goal of previously reported works by us [5–7]. Even though the studies were limited at the basic coordination chemistry stage, the choice of the ligands fell into the active drug families (for instance, 6-thiopurine, H₂tp, an anti-leukemic drug, see Ref. [5] and references therein; piroxicam, an anti-inflammatory drug, see Ref. [8] and references therein), and into some biomolecules or their fragments (adenosine 5'-phosphates: atp [9], adp [10]; imidazole, pyrimidine and thiazole derivatives [6,11]). Such ligands were selected because some of their metal complexes were previously reported (see for instance, Refs. [12,13] and references therein) as having interesting pharmaceutical activities.

We therefore thought that it was worth continuing the synthetic and structural investigation on ruthenium-complexes with imidazole, purine and pyrimidine derivatives and to analyze the physicochemical properties of the new species. The study reported in this paper has

also been oriented at the understanding of C–H···Cl and C–H···N interactions because reaction mechanisms in every area of chemistry and biochemistry are tuned by subtle structural effects often related to a variety of weak forces, which are usually not well known and sometimes completely ignored. It has to be recalled that during recent years the investigation of weak X–H···Y hydrogen bond type interactions (X = C; Y = N, O, S, Cl, π -systems) or agostic type interactions (X = C, N; Y = metal center) has acquired much interest [14]. Finally we wish to note that the Ru–Sb coordination chemistry is far less known and abundant than the corresponding ones relevant to Ru–P and Ru–As linkages; nevertheless, it has recently been reported that Rh/Ru–SbPh₃ derivatives have a promising new coordination and organometallic chemistry, relevant to bioinorganic oriented ligands [5,14f,14g]. These facts have provoked curiosity on species containing the Ru–Sb function and imidazole and pyrimidine derivatives. This encouraged us to find that the reaction of *trans*-[RuCl₂(SbPh₃)₄] [15] with excess methylimidazole (Meim, see Scheme 1 for the numbering of the atoms used throughout the paper) and methylpyrimidine (Mepym) in chloroform/ethanol produced [RuCl₂L₂(SbPh₃)₂] with a *cis* arrangement of the L ligands.

2. Experimental

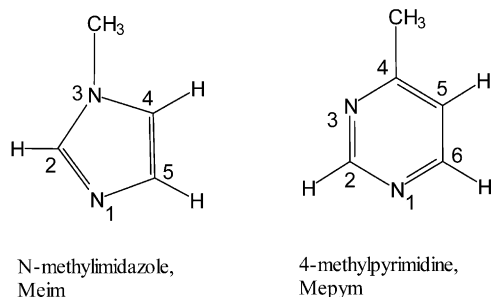
2.1. Materials

Reagent grade RuCl₃·3H₂O, SbPh₃, PPh₃, *N*-methylimidazole, 4-methylpyrimidine, and 1,3-thiazole were obtained from Aldrich and used without any further purification.

2.2. Synthesis

2.2.1. *trans*-[RuCl₂(SbPh₃)₄] (**1**)

The compound was prepared as previously reported in Ref. [15] through a modification reported in Ref. [5].



Scheme 1. Representation of the numbering used throughout the paper for the Meim and Mepym ligands.

2.2.2. *trans,cis,cis*-Dichlorobis(*N*-methylimidazole)bis(triphenylstibine)ruthenium(II) ethanol solvate, $[RuCl_2(Meim)_2(SbPh_3)_2] \cdot CH_3CH_2OH$ ($2 \cdot CH_3CH_2OH$), and *trans,cis,cis*-dichlorobis(*N*-methylimidazole)bis(triphenylstibine)ruthenium(II) ethylacetate solvate, $[RuCl_2(Meim)_2(SbPh_3)_2] \cdot CH_3COOCH_2CH_3$ ($2 \cdot CH_3COOCH_2CH_3$)

80 mg (0.05 mmol) of **1** were dissolved in $CHCl_3$ (8 ml) previously deaerated by flushing ultrapure nitrogen. The dark red magenta solution was added of excess Meim, 50 mg (0.6 mmol). The mixture was refluxed under stirring and in an atmosphere of nitrogen for 3 h. A brown orange solution was obtained. The solution was evaporated under vacuum, in a stream of nitrogen, to dryness. The solid residue was treated with Et_2O (10 ml) previously deaerated under nitrogen and the mixture was stirred for 0.5 h. A suspension containing a pink crystalline solid formed; it was filtered off under nitrogen, rinsed with deaerated $EtOH/Et_2O$ (1:10) and then dried and stored under vacuum. Yield 37 mg, 67%. *Anal.* Found: C, 50.61; H, 4.60; N, 5.00. Calc. for $C_{46}H_{48}Cl_2N_4ORuSb_2$ (MW, 1088.4): C, 50.76; H, 4.45; N, 5.15%. UV–Vis: A freshly prepared pale pink solution of $2 \cdot CH_3CH_2OH$ in deaerated CH_2Cl_2 at 25 °C gives absorption at 620 nm (ϵ , $96.2 \text{ cm}^{-1} \text{ dm}^3$), 505 nm (291), 390 nm (820), 300 (15950). After 48 h from the preparation, under the air atmosphere, at 25 °C, the CH_2Cl_2 solution is violet and gives absorption at 555 nm (ϵ , 1690) and 300 nm (2400). IR: Selected strong and sharp absorption bands are at 1528.1, 1479.7, 1429.9, 1103.7, 1066.6, 730.4, 695.6, 463.7 cm^{-1} .

Single crystals of $2 \cdot CH_3COOCH_2CH_3$ suitable for the X-ray diffraction analysis were obtained from a solution of $2 \cdot CH_3CH_2OH$ (20 mg, 0.018 mmol) in deaerated ethyl acetate (5 ml) containing 10 mg of Meim. The solution was first gently warmed to completely dissolve the compound, then it was stored in the refrigerator. Orange crystals formed within 24 h, at 5 °C. Yield, 12 mg; 60%. *Anal.* Found: C, 50.92; H, 4.50; N, 4.90. Calc. for $C_{48}H_{50}Cl_2N_4O_2RuSb_2$ (MW, 1130.4): C, 51.00; H, 4.46; N, 4.96%.

2.2.3. *trans,cis,cis*-Dichlorobis(4-methylpyrimidine)bis(triphenylstibine)ruthenium(II), $[RuCl_2(Mepym)_2(SbPh_3)_2]$ (**3**)

The compound as a yellow microcrystalline powder was prepared through a procedure similar to that reported for **2**, by refluxing (under nitrogen) a mixture of **1** (80 mg, 0.05 mmol), Mepym (54 mg, 0.50 mmol) and deaerated $CHCl_3$ (8 ml). Yield, 36 mg, 68%. *Anal.* Found: C, 52.12; H, 3.58; N, 5.28. Calc. for $C_{46}H_{42}Cl_2N_4RuSb_2$ (MW, 1066.4): C, 51.81; H, 3.97; N, 5.25%. UV–Vis: A freshly prepared orange solution of **3** in deaerated CH_2Cl_2 at 25 °C gives absorption at 600 nm (ϵ , $42.2 \text{ cm}^{-1} \text{ mol}^{-1} \text{ dm}^3$), 500 nm (550), 400 nm (4900), 342 nm (10100). After 48 h from the preparation, under the air atmosphere, at 25 °C, the CH_2Cl_2 solution is green and gives absorption at 591 nm (ϵ , 830) and 338 nm (6250). IR: Selected strong and sharp absorption bands are at 1598.5, 1479.5, 1430.5, 1393.3, 1066.4, 731.0, 695.6, 461.8 cm^{-1} .

Single crystals of **3** as red prisms suitable for the X-ray diffraction experiments were obtained through slow evaporation at 20 °C of a solution of the crystalline powder (30 mg, 0.028 mmol) and Mepym (5 mg) in deaerated ethanol (10 ml). Yield, 20 mg; 65%. *Anal.* Found: C, 52.00; H, 3.72; N, 5.20%.

2.2.4. $[RuCl_2(PPh_3)_3]$ (**4a**) and $[RuCl_2(PPh_3)_4]$ (**4b**)

The compounds were prepared through the procedures previously reported in Ref. [16].

2.2.5. *trans,trans,trans*- $[RuCl_2(Thz)_2(PPh_3)_2]$ (**5**) and *trans,trans,trans*- $[RuCl_2(Mepym)_2(PPh_3)_2]$ (**6**)

The complexes were obtained by the procedures previously reported in Ref. [6].

2.3. X-ray diffraction

2.3.1. $[RuCl_2(Meim)_2(SbPh_3)_2] \cdot CH_3COOCH_2CH_3$ ($2 \cdot CH_3COOCH_2CH_3$)

A well formed orange plate of dimensions $0.50 \times 0.50 \times 0.20 \text{ mm}$ was mounted on a glass fiber and then used for the diffraction study, through a Siemens P4 diffractometer at 20 °C. Accurate cell constants (Table 1) were determined by using the full-matrix least-squares refinement of the values of 34 carefully centered randomly selected reflections ($10 < 2\theta < 40^\circ$). The diffraction data set (8713 reflections) was corrected for Lorentz-polarization, and absorption effects (ψ -scan). The structure solution and refinement were performed through Patterson and Fourier synthesis methods, and full-matrix least-squares cycles. The asymmetric unit contains a complex molecule and a co-crystallized ethylacetate molecule. All the H-atoms were set in calculated positions and allowed to ride on the atoms to which they are bound during the subsequent cycles of refinement. All the not-hydrogen atoms of **2** and the

Table 1
Selected crystal data and structure refinement for *trans,cis,cis*-[RuCl₂(Meim)₂(SbPh₃)₂]·CH₃CO₂CH₂CH₃ (**2**·CH₃CO₂CH₂CH₃) and for *trans,cis,cis*-[RuCl₂(Mepym)₂(SbPh₃)₂] (**3**)

	2 ·CH ₃ CO ₂ CH ₂ CH ₃	3
Empirical formula	C ₄₈ H ₅₀ Cl ₂ N ₄ O ₂ RuSb ₂	C ₄₆ H ₄₂ Cl ₂ N ₄ RuSb ₂
Formula weight	1130.39	1066.31
Wavelength (Å)	0.71073	0.71073
Crystal system, space group	monoclinic, <i>P</i> 2(1)/ <i>c</i> (no. 14)	rhombohedral, <i>R</i> (-3) (no. 148)
Unit cell dimensions		
<i>a</i> (Å)	14.213(3)	27.690(2)
<i>b</i> (Å)	20.376(1)	27.690(2)
<i>c</i> (Å)	16.406(1)	27.690(2)
α (°)	90	118.22(2)
β (°)	91.80(1)	118.22(2)
γ (°)	90	118.22(2)
<i>V</i> (Å ³)	4748.9(11)	7285.5(9)
<i>Z</i>	4	6
<i>D</i> _{calc} (Mg m ⁻³)	1.581	1.458
θ Range for data collection (°)	1.75–25.00	1.89–25.00
Reflections collected	8713	8837
Reflections unique	8354 [<i>R</i> _{int} = 0.0126]	8268 [<i>R</i> _{int} = 0.0268]
Refinement method	Full-matrix least-squares on <i>F</i> ²	Full-matrix least-squares on <i>F</i> ²
Data/restraints/parameters	8354/0/513	8268/0/487
Final <i>R</i> indices [<i>I</i> > 2σ(<i>I</i>)]	<i>R</i> ₁ = 0.0460, <i>wR</i> ₂ = 0.1171	<i>R</i> ₁ = 0.0435, <i>wR</i> ₂ = 0.0816
<i>R</i> indices (all data)	<i>R</i> ₁ = 0.0554, <i>wR</i> ₂ = 0.1246	<i>R</i> ₁ = 0.0891, <i>wR</i> ₂ = 0.0971

oxygen atoms of CH₃CO₂CH₂CH₃ were treated as anisotropic, whereas all the H-atoms and the carbon atoms of ethyl acetate were treated as isotropic.

All the calculations were performed by using the SHELX 97 [17], and PARST 97 [18], whereas the graphics outputs were obtained through the X-PRIME-ZORTEP [19] and ORTEP32 [20] packages implemented on PC-Pentium machines.

2.3.2. [RuCl₂(Mepym)₂(SbPh₃)₂] (**3**)

A well formed red prism of dimensions 0.40 × 0.15 × 0.15 mm was mounted on a glass fiber and used for the diffraction study at 20 °C. Accurate cell constants (Table 1) were determined by using the values of 24 carefully centered randomly selected reflections from the range 8 < 2θ < 18°. The diffraction data set (8837 reflections) was corrected as reported above for the Meim derivative. The asymmetric unit contains a complex molecule. All the H-atoms were set in calculated positions and allowed to ride on the atoms to which they are bound. All the not-hydrogen atoms were treated as anisotropic whereas all the H-atoms were

treated as isotropic. The assignment of the N(3) and C(5) atoms for the two Mepym ligands has been based first on the comparative analysis of the thermal parameters, the bond distances and bond angles, and on the agreement factors computed for the four possible models which can be obtained by alternating the two atoms in both the Mepym moieties. A second check was based on the possible hydrogen bonds involve the N(3) atoms as H-acceptors and the C(5) atoms as hydrogen donors.

All the methods for data reduction and structure solution and refinement, machines and computer programs were as those described above for the structure of **2**·CH₃CO₂CH₂CH₃.

2.4. Spectroscopy

The ¹H NMR mono-dimensional and bidimensional COSY and NOESY spectra were recorded in CDCl₃ solution at 25.0 ± 0.5 °C (concentration of the complex molecule, 0.01 mol dm⁻³) through a Brücker Advance DRX 600-14 Tesla spectrometer operating at 600 MHz.

The IR spectra were obtained through a Perkin–Elmer 1600 FT–IR spectrometer by using the KBr pellet technique.

The UV–Vis spectra were recorded in CH₂Cl₂ solution at 25.0 ± 0.5 °C (concentration of the complex molecule, ranges 6.43 × 10⁻³–4.15 × 10⁻⁵ mol dm⁻³) through a Perkin–Elmer EZ101 spectrometer in the range 1100–190 nm.

2.5. Electrochemistry

Materials and apparatus for electrochemistry measurements are as previously described [21]. Unless otherwise specified, all potential values are referred to the saturated calomel electrode (SCE).

2.6. Density functional analysis

All the density functional calculations have been performed by using the GAUSSIAN98/RevA.7 [22] package implemented on an Origin 3800 SG machine at CINECA (Inter-University Computing Center, Casalecchio di Reno, Bologna, Italy). Geometry optimizations, population analysis and vibrational frequencies calculations have been obtained by using the Becke3-LYP method [23] and the LANL2DZ [23] basis set for all the atoms, unless otherwise specified (see below). The models analyzed were: *trans*-[RuCl₂(SbH₃)₄] (**A**), for *trans*-[RuCl₂(SbPh₃)₄]; *head-to-head* and *head-to-tail* *trans,cis,cis*-[RuCl₂(Im)₂(SbH₃)₂], Im = 1,3 imidazole (**B** and **C**), for the rotamers relevant to *trans,cis,cis*-[RuCl₂(Meim)₂(SbPh₃)₂]; *head-to-head* and *head-to-tail* *trans,trans,trans*-[RuCl₂(Im)₂(SbH₃)₂] (**D** and **E**); *head-to-tail* *trans,cis,cis*-[RuCl₂(Im)₂(PH₃)₂] (**F**); *head-to-*

head trans,trans,trans-[RuCl₂(Im)₂(PH₃)₂] (**G**); [Ru(Im)]²⁺ (**H**); Pym = 1,3-pyrimidine (**I**); Pym...Pym (**J**). The model **A** was analyzed by using the 6-31G** basis set for the Cl and H atoms. The models **I** and **J** were computed by using the 6-31G** basis set for all the atoms both through the density functional Becke3LYP method (geometry optimization) and the ab initio CCSD(T) method [23] (single point calculation on the previously optimized coordinates). All the model molecules have been considered at their singlet state, excluding the model **H** which was computed at the triplet state as the singlet and quintet states did not converge. The geometrical parameters have been fully optimized without symmetry constraints except that all the Sb–H bond distances, and all the Ru–Sb–H bond angles within each molecule have been restrained to refine to the same value, respectively, and except the **H** model which was restrained to be planar. The optimization of the geometry was carried out up to the criteria implemented in GAUSSIAN98 (for maximum force and rms force shifts, 0.000450, 0.000300 Hartrees/Bohrs, respectively; and for maximum displacement and rms displacement 0.001800, 0.001200 Å, respectively). For a detailed description of the starting conditions used for each molecule, see Section 3. The analysis for the vibrational frequencies was carried out for the **A**, **C** and **H** model molecules only for reducing computational costs. No imaginary frequency was computed.

Molecular drawings for the optimized models were obtained through XPMa-ZORTEP [19] and ORTEP32 [20] packages (see Section 2.3).

3. Results and discussion

3.1. X-ray crystallography

Selected bond distances and angles for **2**·CH₃COOCH₂CH₃ and **3** are reported in Table 2, whereas the tri-dimensional drawings of the asymmetric units for the two compounds are represented in Figs. 1 and 2. Both the complex molecules **2** and **3** have a pseudo-octahedral coordination sphere which consists of two chloride ions *trans* to each other, two antimony atoms (*cis*) and two nitrogen atoms (N¹, *cis*) from the two Meim and Mepym ligands. The Ru–Cl bond distances (average: 2.4265(12), **2**; 2.4233(17) Å, **3**) are equal for the two compounds and in perfect agreement with the values previously reported for **1** [15] and for *trans,cis*-[RuCl₂(Me₂tp)(SbPh₃)₂] (Me₂tp = 1,9-dimethyl-6-thiopurine) [5]. Slightly smaller values for the Ru–Cl bond distances have been found for [RuCl₂(PPh₃)₃] (average, 2.387(7) Å [24]), for *trans,cis,cis*-[RuCl₂(DMSO)₂(NH₃)₂] (average, 2.407(1) Å [25]) and for *trans,trans,trans*-[RuCl₂(DMSO)₂(Meim)₂] (average, 2.416(3) Å [26]). It has to be recalled that

Table 2

Selected bond lengths (Å) and angles (°) for *trans,cis,cis*-[RuCl₂(Meim)₂(SbPh₃)₂]·CH₃CO₂CH₂CH₃ (**2**·CH₃CO₂CH₂CH₃), and for *trans,cis,cis*-[RuCl₂(Mepym)₂(SbPh₃)₂] (**3**)

	2 ·CH ₃ CO ₂ CH ₂ CH ₃	3
Ru(1)–N(11)	2.111(4)	2.130(5)
Ru(1)–N(21)	2.105(4)	2.132(5)
Ru(1)–Cl(1)	2.4274(12)	2.4291(17)
Ru(1)–Cl(2)	2.4256(12)	2.4175(17)
Ru(1)–Sb(1)	2.5731(5)	2.5816(7)
Ru(1)–Sb(2)	2.5729(7)	2.5701(7)
Sb(1)–C(111)	2.135(5)	2.133(6)
Sb(1)–C(121)	2.153(5)	2.140(6)
Sb(1)–C(131)	2.153(5)	2.143(6)
Sb(2)–C(211)	2.135(5)	2.144(6)
Sb(2)–C(221)	2.141(5)	2.128(8)
Sb(2)–C(231)	2.148(5)	2.123(8)
N(11)–C(12)	1.307(7)	1.326(8)
N(11)–C(15)	1.381(7)	
N(11)–C(16)		1.338(8)
C(12)–N(13)	1.332(7)	1.343(8)
N(13)–C(14)	1.352(8)	1.335(10)
C(14)–C(15)	1.368(8)	1.362(10)
C(15)–C(16)		1.366(9)
N(13)–C(13M)	1.482(8)	
C(14)–C(14M)		1.506(10)
N(21)–C(22)	1.320(6)	1.325(8)
N(21)–C(25)	1.377(6)	
N(21)–C(26)		1.331(8)
C(22)–N(23)	1.342(6)	1.329(8)
N(23)–C(24)	1.363(7)	1.325(9)
C(24)–C(25)	1.356(8)	1.378(10)
C(25)–C(26)		1.354(9)
C(23M)–N(23)	1.452(7)	
C(24)–C(24M)		1.519(11)
Sb(2)–Ru(1)–Sb(1)	98.613(18)	98.03(2)
Cl(1)–Ru(1)–Sb(1)	91.53(3)	94.94(4)
Cl(2)–Ru(1)–Sb(1)	89.15(3)	84.68(5)
Cl(1)–Ru(1)–Sb(2)	88.63(3)	84.49(5)
Cl(2)–Ru(1)–Sb(2)	93.57(3)	96.12(5)
N(11)–Ru(1)–Sb(1)	173.47(11)	172.07(14)
N(21)–Ru(1)–Sb(1)	90.33(11)	89.85(14)
N(11)–Ru(1)–Sb(2)	87.90(11)	88.00(14)
N(21)–Ru(1)–Sb(2)	170.89(11)	170.31(14)
Cl(2)–Ru(1)–Cl(1)	177.58(5)	179.33(6)
N(11)–Ru(1)–Cl(1)	89.05(11)	90.75(15)
N(21)–Ru(1)–Cl(1)	89.40(11)	89.24(15)
N(11)–Ru(1)–Cl(2)	90.01(11)	89.57(15)
N(21)–Ru(1)–Cl(2)	88.27(11)	90.20(15)
N(21)–Ru(1)–N(11)	83.18(15)	84.7(2)
C(111)–Sb(1)–Ru(1)	120.45(14)	120.19(17)
C(121)–Sb(1)–Ru(1)	122.18(13)	112.36(18)
C(131)–Sb(1)–Ru(1)	115.31(13)	123.89(16)
C(211)–Sb(2)–Ru(1)	111.70(13)	112.30(17)
C(221)–Sb(2)–Ru(1)	120.75(14)	123.0(2)
C(231)–Sb(2)–Ru(1)	125.11(14)	119.21(19)
C(12)–N(11)–Ru(1)	124.1(3)	120.5(5)
C(15)–N(11)–Ru(1)	129.3(3)	
C(16)–N(11)–Ru(1)		124.1(4)
C(22)–N(21)–Ru(1)	129.7(3)	119.3(4)
C(25)–N(21)–Ru(1)	124.5(3)	
C(26)–N(21)–Ru(1)		125.2(4)
C(111)–Sb(1)–C(121)	98.56(19)	98.5(2)
C(111)–Sb(1)–C(131)	98.4(2)	99.3(2)

Table 2 (Continued)

	2·CH ₃ CO ₂ CH ₂ CH ₃	3
C(131)–Sb(1)–C(121)	97.0(2)	97.8(3)
C(211)–Sb(2)–C(221)	99.00(19)	99.6(3)
C(211)–Sb(2)–C(231)	99.21(18)	98.8(3)
C(221)–Sb(2)–C(231)	96.3(2)	99.8(3)
C(12)–N(11)–C(15)	106.5(4)	
C(12)–N(11)–C(16)		115.4(6)
C(12)–N(13)–C(14)	107.5(5)	116.6(7)
C(12)–N(13)–C(13M)	125.9(6)	
C(14)–N(13)–C(13M)	126.6(5)	
N(11)–C(12)–N(13)	111.5(5)	126.5(7)
N(13)–C(14)–C(14M)		115.9(8)
C(15)–C(14)–C(14M)		123.6(8)
N(13)–C(14)–C(15)	107.0(5)	120.4(7)
C(14)–C(15)–C(16)		119.1(8)
C(14)–C(15)–N(11)	107.6(5)	
C(15)–C(16)–N(11)		121.8(7)
C(22)–N(21)–C(25)	105.8(4)	
C(22)–N(21)–C(26)		115.5(6)
C(22)–N(23)–C(24)	107.9(4)	117.4(7)
C(22)–N(23)–C(23M)	126.6(5)	
C(24)–N(23)–C(23M)	125.5(5)	
N(21)–C(22)–N(23)	110.8(4)	126.2(7)
N(23)–C(24)–C(24M)		117.1(8)
C(25)–C(24)–C(24M)		122.8(8)
C(25)–C(24)–N(23)	106.0(4)	120.1(7)
C(26)–C(25)–C(24)		118.4(7)
C(24)–C(25)–N(21)	109.5(5)	
C(25)–C(26)–N(21)		122.4(7)

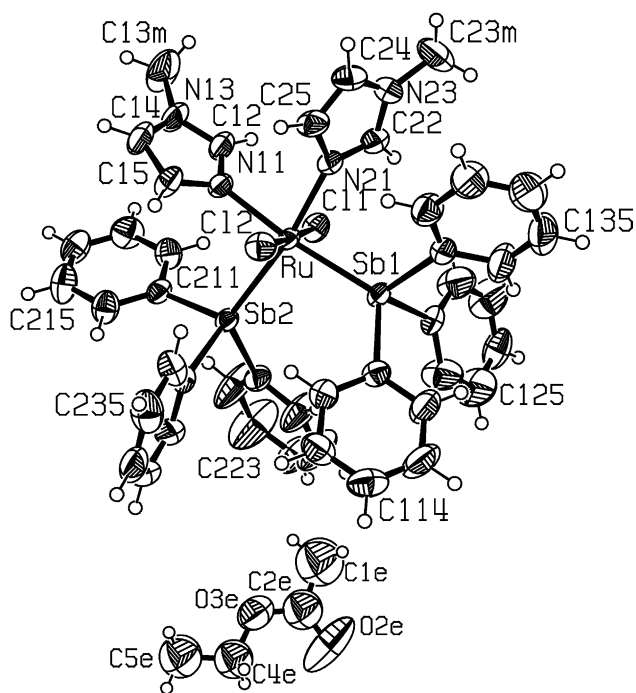


Fig. 1. Drawing of the molecules of the asymmetric unit for *trans,cis,cis*-[RuCl₂(Meim)₂(SbPh₃)₂]·CH₃CO₂CH₂CH₃ (2·CH₃CO₂CH₂CH₃). The ellipsoids enclose 30% probability. The labeling for some of the atoms from the phenyl rings is omitted for the sake of clarity.

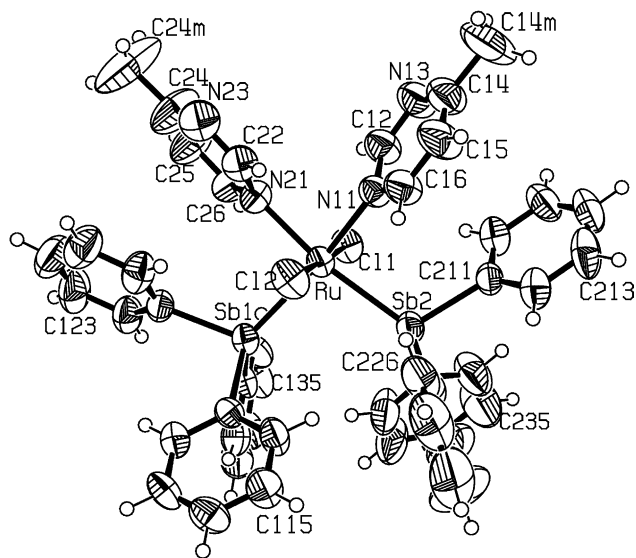


Fig. 2. Drawing of the molecule *trans,cis,cis*-[RuCl₂(Me-pym)₂(SbPh₃)₂] (3). The ellipsoids enclose 30% probability. The labeling for some of the atoms from the phenyl rings are omitted for the sake of clarity.

weaker Ru–Cl bonds can facilitate the removal of one Cl[−] anion from the metal, which was recognized as a crucial step in the cytostatic processes exerted by metal complexes [27]. The Ru–Sb bond distances (average: 2.5730(5), **2**; 2.5758(7) Å, **3**) are significantly smaller than the value found for **1** (average, 2.6295(6) Å) [15] and in agreement with the values found for *trans,cis*-[RuCl₂(Me₂tp)(SbPh₃)₂] (2.572(1) Å) [5]. The Ru–N bond distances (average: 2.108(4), **2**; 2.131(5) Å, **3**) are shorter than the value found for Ru–N(7) (2.157(10) Å) in *trans,cis*-[RuCl₂(Me₂tp)(SbPh₃)₂] [5], but are in agreement with the corresponding values found for [Ru(Meim)₆]²⁺ (in the range, 2.095(4)–2.107(4) Å [28]) and for *cis*-[Ru(H₂O)(Bipy)₂(Meim)]²⁺ (Meim *trans* to N, 2.081(6) [29]) and for *trans,trans,trans*-[RuCl₂(DM-SO)₂(Meim)₂] (2.104(3) Å [26]). It is noteworthy that for *trans*-[RuCl₂(PPh₃)(Thz)₃] the two Ru–N(*trans* to N) bond distances average 2.094(5) Å [6] whereas the Ru–N(*trans* to P) bond distance is much longer, 2.183(5) Å. This fact means that the *trans* influence exerted by triphenylstibine on N(imidazole) is significantly smaller than that by triphenylphosphine at least for this class of octahedral ruthenium(II) complexes, thus explaining the preference for the *cis* isomer over the *trans* one found for **2** and **3**. The bond angles at the metal center deviate significantly from the idealized values of 90 and 180°. In fact the smallest values for the couples of *cis* atoms are those relevant to the N(11)–Ru–N(21) angles (83.18(15)°, **2**; 84.7(2)°, **3**); whereas the largest values are, as expected, those for Sb(1)–Ru–Sb(2) (98.613(18)°, **2**; 98.03(2)°, **3**).

3.2. Triphenylstibine ligands

The Sb–C bond distances are normal and in the range 2.135(5)–2.153(5) Å, **2**, and 2.123(8)–2.144(6) Å, **3** (the average value being 2.140 Å on all 12 values, in agreement with the mean value of 2.158 found for **1**) [15]. The Ru–Sb–C bond angles are in the wide ranges 111.70(13)–125.11(14)°, **2**, and 112.30(17)–123.89(16)°, **3**. On the contrary, the C–Sb–C bond angles are within the narrow range 97.0(2)–99.8(3)° (similar trends have been found for **1** [15]), in agreement with a smaller *cone angle* [30] for SbPh₃ when compared to PPh₃. These facts suggest that relatively small energy barriers are required to change the M–Sb–C angle by rotating the M–Sb vector around the SbPh₃ group, and that the steric contribution for the dissociative reactions is smaller for the SbPh₃ derivatives when compared to the PPh₃ species. Furthermore, it has to be noted that the smallest Ru–Sb–C angle for **2** is relevant to the C(211)/C(216) phenyl ring, which is involved in an intramolecular *stacking* interaction with the N(11)/C(15) imidazole ring (dihedral angle between the least-squares planes formed by the two rings, 27.5(3)°; shortest interatomic distance, N(11)···C(211) 3.351(8) Å). The phenyl groups of the SbPh₃ ligands interact with (Ru)Cl chloride donors via C–H···Cl hydrogen bond type interactions. Selected short H···Cl intramolecular contact distances are: C(212)H···Cl(1), 2.94(1) Å and C(236)H···Cl(2), 2.69(1) Å for **2**; C(216)H···Cl(1), 2.95(1) Å; C(226)H···Cl(2), 2.96(1) Å for **3**. Such types of linkages have been previously reported and commented on (see Refs. [14d,14e]).

3.3. Meim ligands

The two Meim ligands of the complex molecule of **2** have the same orientation with respect to the Ru–Cl vectors (namely *head-to-head*). In fact, the C–N(1)–Ru–Cl(1) torsion angles are –30.7(1)° (C(12)) and –31.8(1)° (C(22)) for the two ligands, respectively. The Ru(II) atom deviates (0.122(1) Å) from the plane of N(11)/C(15) but is almost coplanar with the N(21)/C(25) system. This difference has reasonably to be ascribed to the *stacking* interaction presented above (see Section 3.2), which involves the first but not the latter imidazole ring. Interestingly, the two Ru–N(1)–C(2) bond angles differ significantly (124.1(3) and 129.7(3)°); the opposite trend is shown by the two Ru–N(1)–C(5) bond angles (129.3(3) and 124.5(3)°). This fact suggests that the swinging in the plane of the Meim ligand with respect to the Ru–N linkage has a small energy barrier (at least within a small range) and this can play a role in the coordination of the imidazole moiety to metal ions in the biological systems. Differences in the trend of the M–N(1)–C(2) and M–N(1)–C(5) bond angles for some Zn(II)–imidazole complexes reported in the literature

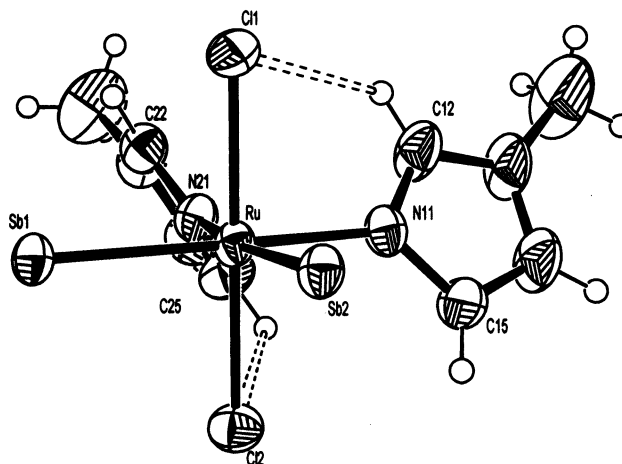


Fig. 3. Representation of the Ru(Meim)₂ moiety of the complex molecule **2** showing the C–H···Cl contacts. The C(12)···Cl(1) contact distance is 3.226(6) Å, whereas the C(15)···Cl(2) distance is 3.367(6) Å. The Ru–N(12)–C(12) angle is 124.1(3)°, smaller than Ru–N(12)–C(15) (129.3(3)°). Similarly, the short C(25)···Cl(2) contact distance is related to the narrow Ru–N(21)–C(25) angle (124.5(3)°). The C–H···Cl attractive interactions tune the bending of Ru–N–C angles.

have been previously noted and commented on [11]. The C(12) atom and the Cl(1) donor are linked by an intramolecular C–H···Cl hydrogen bond type interaction (C···Cl, 3.226(6) Å) in agreement with a narrower Ru–N(11)–C(12) angle, when compared to Ru–N(11)–C(15) (Fig. 3) (C(15)···Cl(2) contact distance, 3.367(6) Å). See Ref. [14c] for previously reported intramolecular C–H···Cl hydrogen bond type interactions as found in Ru–imidazole complexes. The energy barrier required to bend the Ru–N(1)–C(2) bond angle (in plane) was computed (see Section 3.7.1.2).

3.4. Mepym ligands

The two Mepym ligands of the complex molecule **3** have opposite orientation with respect to the Ru–Cl vectors (namely *head-to-tail* orientation; C–N(1)–Ru–Cl(1) torsion angles, 31.5(2)° (C(12)) and –148.4(2)° (C(22)). The Ru atom is coplanar with both the pyrimidine rings. The N(11)/C(16) pyrimidine ring has *stacking* interactions with the C(211)/C(216) phenyl group (shortest interatomic contact distance, N(11)···C(211) 3.366(8) Å; dihedral angle between the planes, 24.7(5)°). A similar *stacking* interaction exists between the N(21)/C(26) pyrimidine system and the C(121)/C(126) phenyl group (shortest contact distance, N(21)···C(121) 3.410(8) Å; dihedral angle between the planes, 25.0(6)°). The *stacking* interactions are probably responsible for the small values of the Ru–Sb(1)–C(121) (112.4(2)°) and Ru–Sb(2)–C(221) (112.3(2)°) bond angles when compared to the other Ru–Sb–C angles. The bond distances within the pyrimidine rings range 1.325(8)–1.343(8) Å (N–C) and 1.354(9)–1.378(10) Å (C–C) and are in agreement with the corresponding

values previously found for *catena*-poly-[(Mepym)copper(I)- μ -thiocyanato-*N*,(μ -*S*)] [31]. The pyrimidine ring bond distances for **3** compare well also with the corresponding values for *trans*-[Pt(NH₃)₂(N⁷-9-ethyl-guanine)(N¹-7,9-dimethylguanine)]²⁺ [32]. The Ru–N(1)–C(2) angles (120.5(5), 119.3(4)°) are smaller than the Ru–N(1)–C(6) ones (124.1(4) and 125.2(4)°) and this is usual for the metal coordinated Mepym ligand [31]. The bond angles C(2)–N(3)–C(4) average 117.0(7)° in agreement with the mean value previously reported for a number of N¹-not-protonated pyrimidine rings of purines (116 ± 3°) [33]. Interestingly, the N(13) atom has an intermolecular C–H···N hydrogen bond type interaction with C(25) (–*y*, –*z*, –*x*) (N···C, 3.582(9) Å; N···H–C, 153(1)°) (Fig. 4); similarly, N(23) interacts with C(15) (–*z*, –*x*, –*y*) (N···C, 3.692(9) Å; N···H–C, 167(1)°). The C–H···N intermolecular interaction between the pyrimidine ligands just discussed suggested to carry out a density functional and ab initio analysis whose preliminary results are reported below.

3.5. ¹H NMR spectroscopy

The spectrum for **2** in CDCl₃ (0.01 M, 25 °C) has peaks at 7.81 ppm (s, 1H, H²), 7.69 (d, 1H, H⁵), 7.36 (d, 6H, H^{o,Ph}), 7.16 (t, 3H, H^{p,Ph}), 7.03 (t, 6H, H^{m,Ph}), 6.48 (d, 1H, H⁴), and 3.28 (s, 3H, H^{Me}), in agreement with bidimensional COSY and NOESY analyses. All the signals relevant to the free Meim ligand (6.91, s, 1H, H²; 6.53, d, 1H, H⁵; 6.40, d, 1H, H⁴; 3.14, s, 3H, H^{Me}) undergo a shift towards lower fields, the larger effects

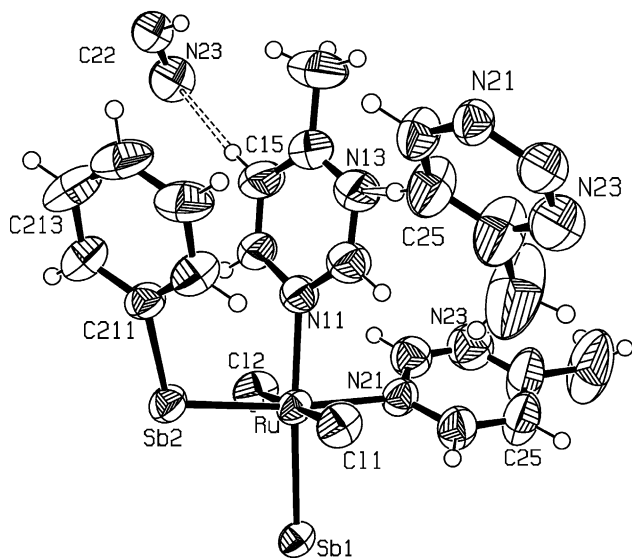


Fig. 4. The diagram shows the selected interactions which involve the Mepym ligand of **3**. Each pyrimidine ring is connected intramolecularly to two other base moieties from symmetry related complex molecules via C–H···N interactions. The C···N contact distances are 3.582(9) and 3.692(9) Å. The drawing also represents the facing between one Mepym ligand and a phenyl ring which stacks intramolecularly.

being those relevant to the H² and H⁵ protons. The latter datum has probably to be ascribed mostly to the metal ligation to N(1), even though the effects due to the intramolecular C–H···Cl interactions play a significant role. It has to be recalled that the N–H···Cl[–] hydrogen bond formation causes a large down field effect (4 ppm) on the signal by the nitrogen-bound proton in a platinum(II)–acridine derivative [34].

The spectrum of **3** in CDCl₃ (0.01 M, 25 °C) has peaks at 9.50 ppm (s, 1H, H²), 9.02 (d, 1H, H⁶), 7.34 (d, 6H, H^{o,Ph}), 7.20 (t, 3H, H^{p,Ph}), 7.04 (t, 6H, H^{m,Ph}), 6.69 (d, 1H, H⁵), and 2.34 (s, 3H, H^{Me}). The signals relevant to H² and H⁶ from Mepym undergo a lower field shift of 0.44 and 0.46 ppm, respectively. On the contrary the doublet relevant to H⁵ undergoes a high field shift by 0.44 ppm. A similar trend happened to the signals from the Mepym protons upon coordination to Ru(II) centers for *trans,trans,trans*-[RuCl₂(Mepym)₂(PPh₃)₂] (CDCl₃) [6]. On decreasing the temperature from 313 K down to 223 K the spectra of **2** and **3** do not change significantly, the largest effect being an up-field shift (0.10 ppm) by the signals from H² and from H^{o,Ph}, in agreement with fast rotations of Meim and Mepym ligands and Ph groups around the Ru–N and Sb–C vectors up to 223 K.

3.6. Electrochemistry

3.6.1. Triphenylstibine derivatives

Fig. 5 compares the cyclic voltammetric behavior of the precursor *trans*-[RuCl₂(SbPh₃)₄] (**1**), with that of *trans,cis,cis*-[RuCl₂(Meim)₂(SbPh₃)₂] (**2**). Both the Ru(II) derivatives display an oxidation process possessing features of chemical reversibility in the cyclic voltammetric time-scale. In both cases, controlled potential coulometry shows the consumption of one electron/molecule, and the exhaustively oxidized solu-

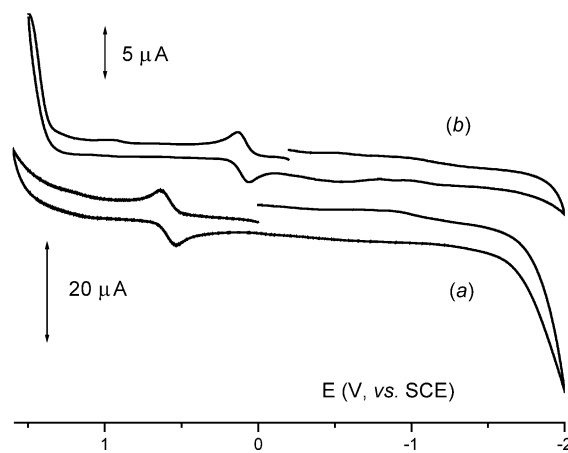


Fig. 5. Cyclic voltammetric responses recorded at a platinum electrode on a CH₂Cl₂ solution containing: (a) **1** (0.5 × 10^{–3} mol dm^{–3}); (b) **2** (0.8 × 10^{–3} mol dm^{–3}). [NBu₄][PF₆] (0.2 mol dm^{–3}) supporting electrolyte. Scan rate 0.2 V s^{–1}.

tions exhibit a cyclic voltammetric profile quite complementary to the original ones, thus testifying the chemical reversibility of the Ru(II)/Ru(III) redox change also in the long times of macro-electrolysis. Upon exhaustive oxidation, the original red–magenta solution of **1** turns orange–brown (in agreement with previous results [15,35,36]), whereas the pink solution of **2** turns blue–gray.

The analysis of the cyclic voltammograms of **1** with scan rate varying from 0.02 to 1.00 V s⁻¹ is diagnostic for a simple quasi-reversible electron transfer in that: (i) the current ratio i_{pc}/i_{pa} is constantly equal to 1; (ii) the current function $i_{pa} \cdot v^{-1/2}$ remains substantially constant; and (iii) the peak-to-peak separation, ΔE_p , progressively increases from 66 to 130 mV [37]. Similar diagnostic parameters also hold for complexes **2** and **3**, even if the ΔE_p values depart less from the theoretical value of 59 mV. In fact, for **2** it increases from 62 to 77 mV and for **3** it increases from 65 to 95 mV. Hence it can be speculated that the molecular strains accompanying the Ru(II)/Ru(III) step are slightly lower for **2** and **3** with respect to **1**.

Table 3 compiles the formal electrode potentials for the oxidation process of the present complexes. From the comparison of the values for **2** and **3** with those for the precursor **1**, it is well evident that both Meim and Mepym are less electron-withdrawing than SbPh₃. In particular, Meim is much more effective than Mepym in addressing electron density towards the Ru(II) core.

Table 3

Formal electrode potentials (V, vs. SCE; values in brackets refer to the Fe/Fe⁺ couple) and peak-to-peak separation (mV) for the reversible oxidation process exhibited by the Ru(II) complexes under study and related derivatives, in dichloromethane solution

Species	E°	ΔE_p^a	Reference
[RuCl ₂ (SbPh ₃) ₄] (1)	+0.59	(+0.20) (+0.18)	83 [15]
[RuCl ₂ (SbMe ₂ Ph) ₄]		(+0.07)	[36]
[RuCl ₂ (Meim) ₂ (SbPh ₃) ₂] (2)	+0.12	(-0.27)	69
[RuCl ₂ (Mepym) ₂ (SbPh ₃) ₂] (3)	+0.47	(+0.08)	73
[RuCl ₂ (PPh ₃) ₃] (4a)	+0.53 ^d	(+0.14)	b
[RuCl ₂ (PPh ₃) ₄] (4b)	+0.67 ^c	(+0.28)	89
[RuCl ₂ (PMe ₃) ₄]		(-0.13)	[36]
[RuCl ₂ (Thz) ₂ (PPh ₃) ₂] (5)	+0.33	(-0.06)	75
[RuCl ₂ (Mepym) ₂ (PPh ₃) ₂] (6)	+0.46	(+0.07)	109
SbPh ₃	+1.47 ^{a,c}		b
PPh ₃	+1.26 ^{a,c}		b
Fe(C ₅ H ₅) ₂	+0.39		85

^a Measured at 0.1 V s⁻¹.

^b Present work.

^c The present oxidation could be due to [RuCl₂(PPh₃)₃]; see text.

^d The present oxidation could be due to RuCl₂(PPh₃)₂ (or to [RuCl₂(PPh₃)₂]); see text.

^e Peak potential for irreversible processes.

3.6.2. Triphenylphosphine derivatives

Like the related triphenylstibine complexes, *trans,trans*-[RuCl₂(Thz)₂(PPh₃)₂] (**5**) and *trans,trans*-[RuCl₂(Mepym)₂(PPh₃)₂] (**6**) [6] exhibit a Ru(II)/Ru(III) oxidation. Really, concerned with complex **6**, the oxidation process results partially chemically reversible, in that cyclic voltammetry on its exhaustively oxidized solution reveals the presence of only minor amounts of the corresponding mono-cation. In contrast, the anodic process for **5** is completely reversible; in fact, the yellow solution of **5** assumes a golden color upon exhaustive oxidation and exhibits a cyclic voltammetric profile complementary to the original one.

To better account for the electronic effects of the ligands for **5** and **6**, the electrochemical behavior of [RuCl₂(PPh₃)₃] (**4a**), and *trans*-[RuCl₂(PPh₃)₄] (**4b**), has been investigated, as to the best of our knowledge, such information is lacking (likely due to the fact that the chemical relationships between **4a** and **4b** in non-aqueous solution are still unresolved). Based on spectroscopic data it has been proposed that **4b** completely dissociates to [RuCl₂(PPh₃)₃]+PPh₃ [38], whereas **4a** partially dissociates (less than 20%) to [RuCl₂(PPh₃)₂]₂ (or RuCl₂(PPh₃)₂+PPh₃ [38,39]. The existence (in solution) of [RuCl₂{P(OPh)₃}₄] [40], [RuCl₂(PPhH₂)₄] [35] and [RuCl₂(PPh₂H)₄] [41], even taking into account of the prohibitive steric repulsions, makes the proposed complete non-existence in solution of **4b** to be considered cautiously. Thus it seemed useful to look at the problem. Fig. 6 illustrates the cyclic voltammetric response of an analytically pure sample of [RuCl₂(PPh₃)₄] (**4b**), dissolved in dichloromethane solution. The overall profile exhibited by the original orange solution (Fig. 6(a)) shows a first oxidation (possessing partial chemical reversibility) followed by a further

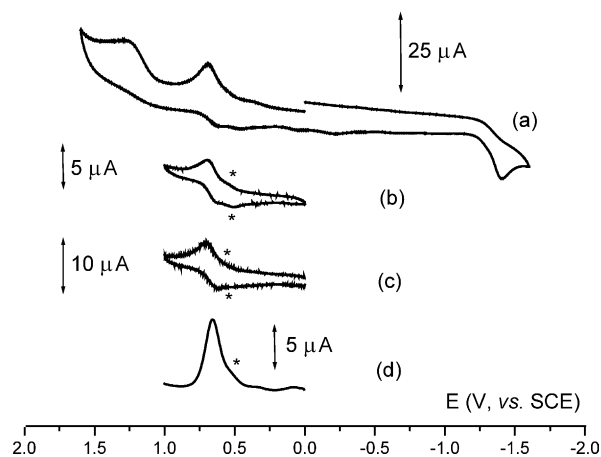
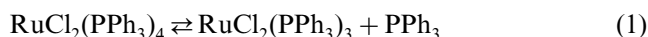


Fig. 6. Cyclic (a–c) and OSWV (d) voltammograms recorded at a platinum electrode on a CH₂Cl₂ solution containing **6** (0.6×10^{-3} mol dm⁻³). [NBu₄][PF₆] (0.2 mol dm⁻³) supporting electrolyte. Scan rates: (a, c) 0.2 V s⁻¹; (b) 0.02 V s⁻¹; (d) 0.1 V s⁻¹.

irreversible oxidation occurring at potential values ($E_p = +1.28$ V) essentially coincident with that of free PPh_3 . An irreversible reduction occurs at rather negative potential values ($E_p = -1.44$ V), which we assign to the Ru(II)/Ru(0) process. Indeed, analysis of the first anodic step (Fig. 6(b,c)) reveals (particularly at low scan rates) the presence of a peak-system (starred) preceding the main process, which even in square wave voltammetry is unresolved (Fig. 6(d)). Based on the above cited knowledge of the solution behavior of **4b**, we can preliminarily state that a chemical equilibrium between two redox active species is operative, and the scan rate can compete with its setting up. The effect exerted by the increase of the scan rate is similar to that obtained upon addition of free PPh_3 . As a matter of fact, the effect of the progressive addition of free PPh_3 to a 1:2 mixture of **4a** and **4b** is represented in Fig. 7. The original orange solution gives rise to an overall voltammetric picture (Fig. 7(a)), similar to that illustrated in Fig. 6(a), but for the fact that the two almost overlapping oxidations are now more pronounced and sufficiently well resolved in square wave voltammetry (Fig. 7(a,b)). The progressive addition of PPh_3 causes the first anodic step to disappear (Fig. 7(c,d)). Concomitantly the solution turns brown (microcrystalline **4b** is brown). Such results could be explained, at first instance, on the basis of the equilibrium:



and assigning the first oxidation to $[\text{RuCl}_2(\text{PPh}_3)_3]$ ($E^{\circ'} = +0.53$ V) and the second wave to $[\text{RuCl}_2(\text{PPh}_3)_4]$ ($E^{\circ'} = +0.67$ V).

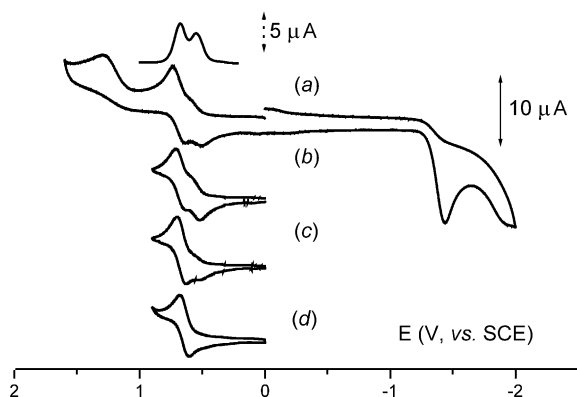


Fig. 7. Cyclic (solid line) and OSWV (dashed line) voltammograms recorded at a platinum electrode on a CH_2Cl_2 solution containing 1:2 mixture of $[\text{RuCl}_2(\text{PPh}_3)_3]$ (0.25×10^{-3} mol dm^{-3}) and $[\text{RuCl}_2(\text{PPh}_3)_4]$ (0.5×10^{-3} mol dm^{-3}). (a, b) Original solution; (c) after the addition of PPh_3 in a 1:1 ratio; (d) after the addition of an excess of PPh_3 in a 1:3 ratio. $[\text{NBu}_4][\text{PF}_6]$ (0.2 mol dm^{-3}) supporting electrolyte. Scan rates: (a) 0.5 V s^{-1} ; (b–d) 0.05 V s^{-1} . OSWV: 0.1 V s^{-1} .

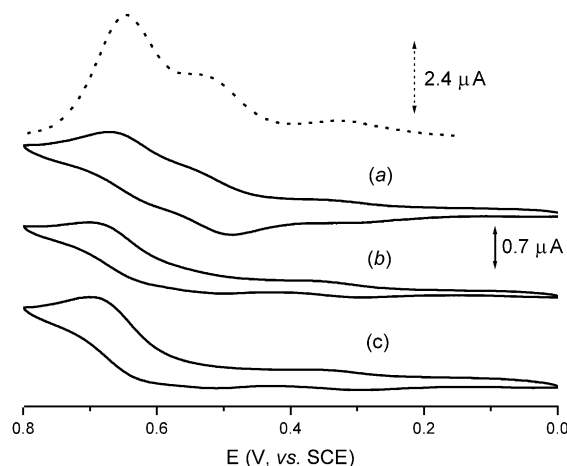


Fig. 8. Cyclic (solid line) and OSWV (dashed line) voltammograms recorded at a platinum electrode on a CH_2Cl_2 solution containing $[\text{RuCl}_2(\text{PPh}_3)_3]$ (0.8×10^{-3} mol dm^{-3}). (a) Original solution; (b) after the addition of PPh_3 in a 1:1 ratio; (c) after the addition of an excess of PPh_3 in a 1:3 ratio. $[\text{NBu}_4][\text{PF}_6]$ (0.2 mol dm^{-3}) supporting electrolyte. Scan rate 0.02 V s^{-1} . OSWV: 0.1 V s^{-1} .

The effect by the progressive addition of PPh_3 to a solution of **4a** when analyzed via cyclic voltammetry is pictured in Fig. 8. In fact, the two essentially overlapping chemically reversible oxidations are again present and the addition of PPh_3 causes the qualitative effects above discussed for **4b**. The only significant difference is that the reversibility of the final process is not complete for **4a**, and that the original orange solution turns yellow upon addition of PPh_3 (the presence of a minor peak-system at about $+0.35$ V, which is unaffected by the addition of PPh_3 , seems to be due to a by-product, rather than to a product arising from equilibria). In the light of the hypothesized equilibrium (Eq. (1)), such a behavior could be due to the fact that in solution **4a** also affords a mixture of **4a** and **4b**. In conclusion, the present voltammetric patterns do not allow a rigorous solution of the dilemma. As a matter of fact, the two almost overlapping oxidations can be assigned either to the mentioned equilibrium **4a/4b** (Eq. (1)), or to the equilibrium **4a**/ $[\text{RuCl}_2(\text{PPh}_3)_2]_2$, assuming in the last case the complete dissociation of **4b**. Unfortunately, attempts to isolate $[\text{RuCl}_2(\text{PPh}_3)_2]_2$ were unsuccessful. This being stated, we note that the values of electrode potentials (Table 3) show that the substitution of PPh_3 ligands with Mepym or Thz makes the Ru(II)/Ru(III) oxidation easier, the Thz substituent being more electron-donating than Mepym.

We finally note that the formal electrode potential of the Ru(II)/Ru(III) couple (a parameter which seems to be related to the biological activity of ruthenium complexes) for **2** ($E^{\circ'} = -0.27$ V, vs. Fc/Fc^+) compares well with that for other ruthenium complexes proved to be effective as anticancer drugs [1k].

3.7. Density functional analysis

3.7.1. Structures of complexes

The optimizations of *head-to-tail trans,cis,cis* and *head-to-tail trans,trans,trans*-[RuCl₂(Im)₂(PH₃)₂] isomers as well as those of the corresponding Thz derivatives were performed at the ZINDO1 [42] semiempirical method level, by using the default parameterization implemented in HyperChem 5.1 [43]. The optimized Ru–Cl bond distances were 2.362 Å in acceptable agreement with experimental values [6]; on the contrary the computed Ru–N (1.953 Å) and Ru–P (2.538 Å) distances are very different from the experimental values (differences in the range 0.130–0.240 Å). For this reason and for the lack of the parameterization for antimony, the faster semiempirical ZINDO1 method was abandoned in favor of the hybrid density functional method at the Becke3LYP/LANL2DZ, /6-31G** levels. The selected geometrical parameters for the model molecules are reported in Tables 4 and 5.

3.7.1.1. [RuCl₂(SbH₃)₄] (A). The calculations were carried out at the Becke3LYP/LANL2DZ level for all the atoms, BS1, and at the Becke3LYP/LANL2DZ level for all the atoms except Cl and H for which extra-basis 6-31G** was used, BS2. A representation of the optimized structure is reported in Fig. 9. The computed (BS2) Ru–Sb bond distances are 2.640 Å (computed infrared parameters: $\nu_{\text{as}}(\text{Ru–Sb})$, 211.0 cm⁻¹; k_{v} , 0.459 mdyne Å⁻¹) in good agreement with the corresponding values found at the solid state for [RuCl₂(SbPh₃)₄] (2.6295(6) Å) [15]. The expected Ru–Sb bond length for the SbPh₃ derivative is higher than that for model A owing to the steric hindrance by the 12 phenyl rings. The computed (BS2) Ru–Cl bond lengths are 2.499 Å (infrared: $\nu_{\text{as}}(\text{Ru–Cl})$, 309.6; k_{v} , 0.807), somewhat larger than the mean value found for [RuCl₂(SbPh₃)₄] at the solid state (2.425(2) Å) [15]. The lengthening for the calculated Ru–Cl distances at BS1 level when compared to the BS2 one was 0.84% (0.021 Å). Similarly, the computed Sb–H bond lengths do not change much

(0.65%, 0.011 Å) on changing the basis set. Furthermore, previously reported computations on imidazole and zinc(II)–imidazole complexes [11] revealed that BS1 led to acceptable structures at a relatively low computational cost. For these reasons the subsequent calculations of the Ru(II)–imidazole models were carried out by using the BS1 set for all the atoms.

3.7.1.2. [Ru(Im)]²⁺ (H). The structure was restrained to planarity and then optimized (Becke3LYP/BS1 level) at the triplet state (singlet and quintuplet states did not converge). The computed Ru–N bond distance is 1.959 Å (infrared: $\nu(\text{Ru–N})$, 301.8; k_{v} , 0.573). The computed Ru–N–C(N) and Ru–N–C(C) bond angles are 126.3 and 125.8°. Subsequently, several structures for [Ru(Im)]²⁺ (triplet) with the Ru–N–C(N) (θ) angle fixed at certain values in the range 118.0–134.0° (step, 2°) were optimized. The energy required to bend the θ angle from the equilibrium value (126.3°) down to 118.0° and up to 134.0° is 4.908 and 4.201 kJ mol⁻¹, respectively. The computed changes for the Ru–N bond lengths are smaller than 0.009 Å on passing from $\theta = 118.0^\circ$ to 134° . These data show that the values of the Ru–N–C angles can be much influenced by weak forces like intramolecular C–H···Cl interactions and stacking interactions, as it happens in the structure of **2** at the solid state. In fact, the computed adduct formation energy (at the Becke3LYP/6-31G** level and in the gas phase) for Im···Cl⁻, through the C(2)–H group, is -46.340 kJ (not corrected for BSSE; see Scheme 2 for the selected computed geometrical parameters of the adduct).

It is noteworthy that in the structures of [Ru(Im)₆]²⁺ and [Ru(Meim)₆]²⁺ [28] the Ru–N–C(N) and Ru–N–C(C) angles have almost the same values for all six ligands.

3.7.1.3. [RuCl₂(Im)₂(SbH₃)₂] and [RuCl₂(Im)₂(PH₃)₂]. The isomers/rotamers investigated at the Becke3LYP/BS1 level for all the atoms were *head-to-head trans,cis,cis*- (**B**) (Fig. 10), *head-to-tail*

Table 4
Selected bond lengths (Å) of selected complex models calculated at the Becke3LYP/LANL2DZ level

Molecule	Ru–Sb/P	Ru–Cl	Ru–N	Sb/P–H	N(1)–C(2)	C(2)–N(3)	N(1)–C(5)/C(6)
[RuCl ₂ (SbH ₃) ₄]	2.640	2.499		1.691			
<i>trans,cis,cis</i> -[RuCl ₂ (Im) ₂ (SbH ₃) ₂]	2.637 [2.634]	2.543 [2.544]	2.118 [2.116]	1.707 [1.707]	1.342 [1.342]	1.375 [1.375]	1.402 [1.402]
<i>trans,trans,trans</i> -[RuCl ₂ (Im) ₂ (SbH ₃) ₂]	2.636 [2.637]	2.529 [2.544]	2.130 [2.131]	1.707 [1.708]	1.343 [1.344]	1.375 [1.375]	1.404 [1.404]
[Ru(Im)] ²⁺			1.959		1.398	1.336	1.408
Pym					1.337	1.338	1.339
Pym···pym (H donor)					1.338	1.338	1.340
(H acceptor)					1.339	1.340	1.340

The basis set was expanded to 6-31G** for the Cl and H atoms of [RuCl₂(SbPh₃)₄]. The parameters are relevant to the *head-to-head* rotamers; those relevant to the *head-to-tail* rotamers are given in brackets. Selected data for Pym and Pym···pym adduct as computed at the Becke3LYP/6-31G** level are also reported.

Table 5
Selected bond angles (°) of selected models calculated at the Becke3LYP/LANL2DZ level

Molecule	Sb/P–Ru–Sb/P	Sb/P–Ru–Cl	Sb/P–Ru–N	Cl–Ru–N	N–Ru–N	Ru–N–C(N)	Ru–N–C(C)
[RuCl ₂ (SbH ₃) ₄]	90.0	88.6					
	177.3	91.4					
<i>trans,cis,cis</i> -[RuCl ₂ (Im) ₂ (SbH ₃) ₂]	94.0	88.7	89.4	90.4	87.3	125.9	126.7
	[95.4]	90.3	176.5	90.7			
		[87.2]	[88.9]	[90.9]	[86.8]	[125.7]	[127.0]
		[91.8]	[175.2]	[89.2]			
<i>trans,trans,trans</i> -[RuCl ₂ (Im) ₂ (SbH ₃) ₂]	177.3	88.6	90.0	89.7	179.4	126.1	126.8
		91.4	90.0	90.3			
	[175.6]	[87.8]	[89.8]	[89.2]	[179.9]	[126.4]	[126.6]
		[92.2]	[92.9]	[90.9]			
[Ru(Im)] ²⁺						126.3	125.8

The basis set was expanded to 6-31G** for the Cl and H atoms of [RuCl₂(SbPh₃)₄]. The parameters are relevant to the *head-to-head* rotamers; those relevant to the *head-to-tail* rotamers are given in brackets.

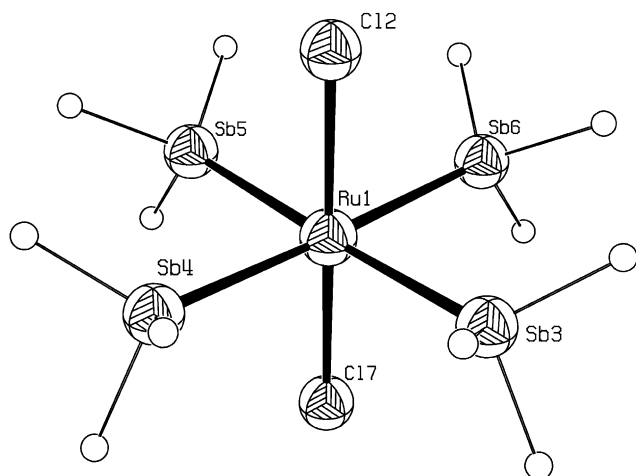
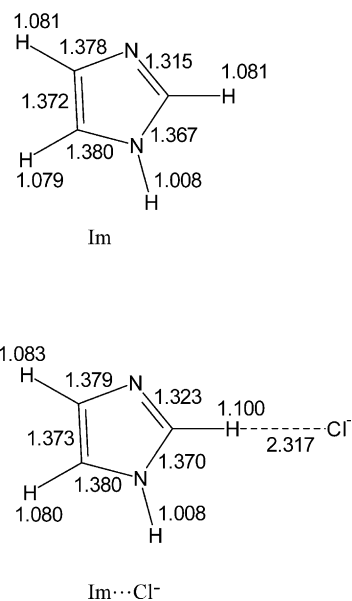


Fig. 9. ORTEP drawing of *trans,cis,cis*-[RuCl₂(SbH₃)₄], model A, as optimized through the GAUSSIAN98/DFT package at the hybrid B3LYP/LANL2DZ (6-31G**, Cl, H) level. The labeling corresponds to the order of the atoms in the Z-matrix and it is the key for the orthogonal atomic coordinates listed in the supporting material.

trans,cis,cis- (C), *head-to-head trans,trans,trans*- (D), and *head-to-tail trans,trans,trans*- (E) for the stibine species, and *head-to-tail trans,cis,cis*- (F) and *head-to-head trans,trans,trans*- (G) for the phosphine species. The goal of the computation for models B–G was to estimate the differences between the electronic energies for the isomers/rotamers, and through this, to roughly estimate their relative stability. It has to be noted that the computed Ru–N distances (2.118–2.130 Å) are in good agreement with the experimental values for **2** (2.108(4) Å). A good agreement (theory/experiment) can also be noted for the Ru–Sb bond distances and for the geometrical parameters within the imidazole ring. The orientation of the imidazole ring around the N–Ru vector in the model molecules B–E (which contains SbH₃ instead of SbPh₃) is influenced mostly by the C–H···Cl interactions (the steric effects are small). As a consequence, the imidazole system is almost eclipsed



Scheme 2. Selected bond lengths for imidazole (Im) and the adduct Im···Cl[−] as computed at the gas phase through the density functional methods at the Becke3LYP/6-31G** level.

with the Ru–Cl bonds (Cl–Ru–N–C torsion angles range 0–2°) and the H···Cl contacts are at a minimum (2.602 Å) for both C(5)–H and C(2)–H. This led to almost equal Ru–N–C(N) and Ru–N–C(C) bond angles (126.7 and 125.9°). The total electronic energy for the four optimized [RuCl₂(Im)₂(SbH₃)₂] isomers differs less than 2.720 kJ mol^{−1} (the *head-to-tail trans,cis,cis* isomers being the most stable). To search for the influence of the Sb/P donor on the difference between the total electronic energy of the isomers, the optimization of the *head-to-tail-trans,cis,cis*- and *head-to-head-trans,trans,trans*-[RuCl₂(Im)₂(PH₃)₂] models (F, G) was also carried out. The difference is small too (3.678 kJ), the *cis* isomer being more stable than the *trans* one. The small difference between the computed energies of the isomers suggests that electronic effects

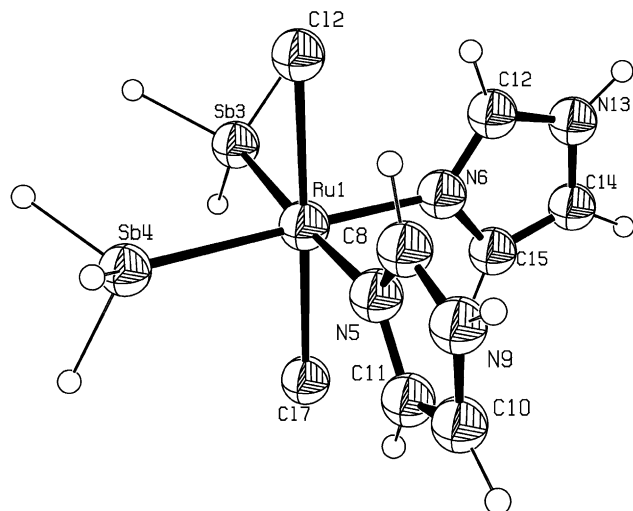
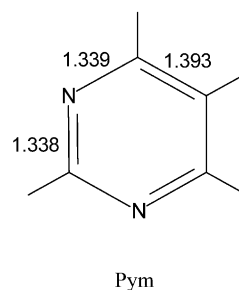


Fig. 10. ORTEP drawing of *head-to-head trans,cis,cis*-[RuCl₂(Im)₂(SbH₃)₂], model **B**, as optimized through the GAUSSIAN98/DFT package at the hybrid B3LYP/LANL2DZ level. The labeling corresponds to the order of the atoms in the Z-matrix and it is the key for the orthogonal atomic coordinates listed in the supporting material.

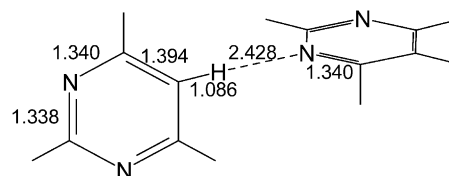
alone do not discriminate the most stable structure, even though one of the *cis* isomers has the smallest energy for the SbH₃-containing model complex (in agreement with the experimental finding at the solid state for **2**). The presence of the bulky phenyl groups in the real molecules reasonably discriminate the stability of the isomers, especially for the PPh₃-containing complexes.

3.7.2. The C–H···N interaction

3.7.2.1. Pym (I) and {Pym···Pym} (J). The starting structure of model **J** had the N(1) atom from one Pym molecule facing the (C(5))H hydrogen atom from a second Pym (pyrimidine) molecule (similar to the Mepym···Mepym pair found at the solid state for **3**). The initial torsion angle C–N···N–C was 40°. All the bond distances were freely refined and each Pym moiety was restrained to be planar. The optimization (at the Becke3LYP/6-31G** level) led to a linear C(5)–H···N(1) arrangement (Scheme 3) in which the N(1)···C(5) contact distance was 3.513 Å, which compares well with the corresponding contact distance found at the solid state for **3** (3.582(9) Å). It has to be noted that C–H···N[−] hydrogen bond type interactions have been previously found and well documented for pyrimidine derivatives [14a,14b]. The computed C–N···N–C torsion angle is 90.0°, which minimizes the repulsion between the hydrogen atoms. The formation energy for the adduct, as computed from the electronic energies without any correction for the basis set superposition error is −11.657 kJ mol^{−1}. An ab initio single point computation at the CCSD(T)/6-31G** level performed on the coordinate sets of models **I** and **J** as



Pym



Pym...Pym

Scheme 3. Selected bond lengths for pyrimidine (Pym) and the adduct Pym···Pym as computed at the gas phase through the density functional methods at the Becke3LYP/6-31G** level.

previously refined through the density functional method Becke3LYP/6-31G** gave an adduct formation energy of −13.891 kJ mol^{−1}, which compares well with the computed value of −18.4 kJ mol^{−1} for the adduct formation between nitromethane and ammonia [44]. These values have to be compared with those previously computed for the formation energy of the base-pairs of the GC-Watson–Crick type (−99.579 kJ mol^{−1}, see Ref. [45] and references therein) and for the formation energy of the adduct between H¹,H⁹-purine-6-thione and H⁹-purine-6-thione(−1) (−116.784 kJ) [14f]. Nevertheless, the role of weak (and often neglected) interactions like those of the C–H···N type can play subtle but important roles in biological systems, at least when hydrophobic pockets are involved.

4. Conclusion

In conclusion, this work showed (first) that [RuCl₂(SbPh₃)₄] is a suitable starting material to prepare *trans,cis,cis*-[RuCl₂L₂L₂] complexes through the reaction with excess (1:10) imidazole and pyrimidine bases under anaerobic conditions. The *cis* substitution instead of *trans* has a rationale in a larger *trans* effect and *trans* influence by triphenylstibine when compared to Meim, Mepym and Cl[−], at least in the case of this type of octahedral complexes. The steric hindrance between the two SbPh₃ ligands is not so severe to force towards the *trans* isomer. Things can be different for the corresponding PPh₃ derivatives because of the larger cone angle by

triphenylphosphine. Both experiments and calculations showed (second) that the Ru–N–C angles for imidazole complexes can change in the range 118–134° at an energy expense not larger than approximately 5 kJ, so that the orientation of the Ru–N vector in the plane of the metal-bound imidazole ring is significantly influenced by weak forces (like C–H···X hydrogen bond type interactions). Both complex molecules **2** and **3** showed (third) a much hydrophobic outer surface and this fact favors the formation of intermolecular C–H···N connections at the solid state. The adduct between two pyrimidine molecules (**3**) via a C(5)–H···N interaction has a computed formation energy (at the gas phase) of $-13.891 \text{ kJ mol}^{-1}$. The analysis of the electrode potentials for the Ru(III)/Ru(II) couple for a series of complexes, showed (fourth) that **2** behaves similarly to known active anticancer compounds; furthermore, the oxidative process is chemically reversible in the long times. Therefore, this type of neutral Ru(II)–imidazole complexes can be easily oxidized to the corresponding Ru(III)–imidazole cations, a form more suitable for transferrin binding and hence for transport processes. The Ru(II) form is instead stable within anoxic environments like cancers. Once one or more nucleobases (for instance, from nucleic acid fragments) have entered the coordination sphere, the kinetically Ru(II) form is stabilized (see E° for **3**). The hybrid density functional analysis at the Becke3LYP/LANL2DZ level was shown (fifth) to be a reliable theoretical tool for reproducing the structure of complexes of the $[\text{RuCl}_2(\text{SbH}_3)_4]$ and $[\text{RuCl}_2(\text{Im})_2\text{L}_2]$ types.

5. Supplementary material

X-ray crystallographic files in CIF format have been deposited with the Cambridge Crystallographic Data Centre, CCDC Nos. 172363 (**2**) and 172364 (**3**). Copies of this information may be obtained free of charge from the Director, CCDC, 12 Union Road, Cambridge CB2 1EZ, UK (fax: +44-1233-336-033; e-mail: deposit@ccdc.cam.ac.uk or www: <http://www.ccdc.cam.ac.uk>).

Acknowledgements

The authors are grateful to Professor Helmut Sigel, University of Basel, for having stimulated their interest in metal complexes with ligands of biological significance, through his papers and lectures. Mr. F. Berrettini is acknowledged for the X-ray data collections at Centro Interdipartimentale di Analisi e Determinazioni Strutturali (CIADS, University of Siena). Centro di Calcolo Interuniversitario per l'Italia del Nord Est (CINECA, Casalecchio di Reno, Bologna), is gratefully acknowledged for the grant project # 00/1038-5 and the use of

the SGI Origin 3800 computer. The authors also thank the University of Siena (PAR 2001), and Consiglio Nazionale delle Ricerche (CNR, Roma) for financial support.

References

- [1] (a) H. Sigel, A. Saha, N. Saha, P. Carloni, L.E. Kapinos, R. Griesser, *J. Inorg. Biochem.* 78 (2000) 129; (b) S.A.A. Sajadi, B. Song, F. Gregán, H. Sigel, *Inorg. Chem.* 38 (1999) 439; (c) S.A.A. Sajadi, B. Song, H. Sigel, *Inorg. Chim. Acta* 283 (1998) 193; (d) E. Freisinger, A. Schimanski, B. Lippert, *J. Biol. Inorg. Chem.* 6 (2001) 378; (e) F. Piccioli, L. Messori, P. Orioli, B. Keppler, E. Alessio, G. Sava, *J. Inorg. Biochem.* (Abstract for the 10th International Conference on Bioinorganic Chemistry) 86 (2001) 379; (f) A.H. Velders, A.C.G. Hotze, G.A. van Albada, J.G. Haasnoot, J. Reedijk, *Inorg. Chem.* 39 (2000) 4073; (g) A.C.G. Hotze, A.H. Velders, F. Ugozzoli, M. Biagini-Cingi, A.M. Manotti-Lanfredi, J.G. Haasnoot, J. Reedijk, *Inorg. Chem.* 39 (2000) 2966; (h) D. Heseck, Y. Inoue, S.R.L. Everitt, H. Ishida, M. Kunieda, M.G.B. Drew, *Inorg. Chem.* 39 (2000) 308; (i) M.J. Clarke, M. Stubbs, in: A. Sigel, H. Sigel (Eds.), *Metal Ions in Biological Systems*, vol. 32 (chapter 21), Marcel Dekker, New York, 1996; (j) L.G. Marzilli, P.A. Marzilli, E. Alessio, *Pure Appl. Chem.* 70 (1998) 961; (k) M.J. Clarke, F. Zhu, D.R. Frasca, *Chem. Rev.* 99 (1999) 2511.
- [2] (a) P.J. Dandliker, M.E. Nunez, J.K. Barton, *Biochem.* 37 (1998) 6491; (b) R.E. Holmlin, M.R. Stemp, J.K. Barton, *Inorg. Chem.* 37 (1998) 29.
- [3] T. Naota, H. Takaya, S.-T. Murahashi, *Chem. Rev.* 98 (1998) 2599.
- [4] (a) W. Peti, T. Pieper, M. Sommer, B.K. Keppler, G. Giester, *Eur. J. Inorg. Chem.* (1999) 1551; (b) G. Sava, I. Capozzi, K. Clerici, G. Gagliardi, E. Alessio, G. Mestroni, *Clin. Exp. Metastasis* 13 (1998) 371.
- [5] C. Bellucci, R. Cini, *J. Inorg. Biochem.* 76 (1999) 243.
- [6] C. Pifferi, R. Cini, *J. Chem. Soc., Dalton Trans.* (1998) 2679.
- [7] R. Cini, R. Bozzi, A. Karaulov, M.B. Hursthouse, A.M. Calafat, L.G. Marzilli, *J. Chem. Soc., Chem. Commun.* (1993) 899.
- [8] R. Cini, *Comments Inorg. Chem.* 22 (2001) 151.
- [9] R. Cini, *Comments Inorg. Chem.* 13 (1992) 1 (and references cited therein).
- [10] R. Cini, C. Pifferi, *J. Chem. Soc., Dalton Trans.* (1999) 699.
- [11] R. Cini, D.G. Musaev, L.G. Marzilli, K. Morokuma, *J. Mol. Struct. (Theochem.)* 392 (1997) 55.
- [12] Q. Zhou, T.W. Hambley, B.J. Kennedy, P.A. Lay, P. Turner, B. Warwick, J.R. Biffin, H.L. Regtop, *Inorg. Chem.* 39 (2000) 3742.
- [13] E. Dubler, in: A. Sigel, H. Sigel (Eds.), *Metal Ions in Biological Systems* (chapter 8), Marcel Dekker, New York, 1996.
- [14] (a) R.K.O. Sigel, E. Freisinger, S. Metzger, B. Lippert, *J. Am. Chem. Soc.* 120 (1998) 12000; (b) M.S. Lüth, E. Freisinger, B. Lippert, *Chem. Eur. J.* 7 (2001) 2104; (c) M. Iwamoto, E. Alessio, L.G. Marzilli, *Inorg. Chem.* 35 (1996) 2384; (d) L.-Y. Huang, U.R. Aulwurm, F.W. Heinemann, F. Knoch, H. Kisch, *Chem. Eur. J.* 4 (1998) 1641; (e) R. Cini, A. Cavaglioni, *Inorg. Chem.* 38 (1999) 3751;

- (f) R. Cini, M. Corsini, A. Cavaglioni, *Inorg. Chem.* 39 (2000) 5874;
- (g) A. Cavaglioni, R. Cini, *J. Chem. Soc., Dalton Trans.* (1997) 1149.
- [15] N.R. Champness, W. Levason, M. Webster, *Inorg. Chim. Acta* 208 (1993) 189.
- [16] (a) T.A. Stephenson, G. Wilkinson, *J. Inorg. Nucl. Chem.* 28 (1966) 945;
- (b) R. Holm (checked by), *Inorg. Synth.* 12 (1970) 238.;
- (c) R. Singler, R.D. Feltham (checked by), *Inorg. Synth.* 12 (1970) 238.
- [17] G.M. Sheldrick, *SHELX 97*, Program for the Refinement of Crystal Structures, University of Göttingen, Göttingen, Germany, 1997.
- [18] M. Nardelli, *PARST 97*, A System of Computer Routines for Calculating Molecular Parameters from Results of Crystal Structure Analyses, University of Parma, Parma, 1997.
- [19] L. Zsolnai, *XPMA-ZORTEP 98*, University of Heidelberg, 1998.
- [20] C.K. Johnson, M.N. Burnett, *ORTEP-3 for Windows*, Oak Ridge National Laboratory, 1998. 32-bit Implementation by L.J. Farrugia, University of Glasgow.
- [21] P. Zanello, F. Laschi, M. Fontani, C. Mealli, A. Ienco, K. Tang, X. Jin, L. Li, *J. Chem. Soc., Dalton Trans.* (1999) 965.
- [22] M.J. Frisch, G.W. Trucks, H.B. Schlegel, G.E. Scuseria, M.A. Robb, J.R. Cheeseman, V.G. Zakrzewski, J.A. Jr. Montgomery, R.E. Stratmann, J.C. Burant, S. Dapprich, J.M. Millam, A.D. Daniels, K.N. Kudin, M.C. Strain, O. Farkas, J. Tomasi, V. Barone, M. Cossi, R. Cammi, B. Mennucci, C. Pomelli, C. Adamo, S. Clifford, J. Ochterski, G.A. Petersson, P.Y. Ayala, Q. Cui, K. Morokuma, D.K. Malick, A.D. Rabuck, K. Raghavachari, J.B. Foresman, J. Cioslowski, J.V. Ortiz, A.G. Baboul, B.B. Stefanov, G. Liu, A. Liashenko, P. Piskorz, I. Komaromi, R. Gomperts, R.L. Martin, D.J. Fox, T. Keith, M.A. Al-Laham, C.Y. Peng, A. Nanayakkara, M. Challacombe, P.M.W. Gill, B. Johnson, W. Chen, M.W. Wong, J.L. Andres, C. Gonzalez, M. Head-Gordon, E.S. Replogle, J.A. Pople, *Gaussian 98*, Revision A.7, Gaussian, Inc., Pittsburgh, PA, 1998.
- [23] A. Frish, M.J. Frisch, *Gaussian 98*, User's Reference, 2nd ed., Gaussian, Inc., Pittsburgh, PA, 1998.
- [24] S.J. La Placa, J.A. Ibers, *Inorg. Chem.* 4 (1965) 778.
- [25] M. Henn, E. Alessio, G. Mestroni, M. Calligaris, W.M. Attia, *Inorg. Chim. Acta* 187 (1991) 39.
- [26] C. Anderson, A.L. Beauchamp, *Can. J. Chem.* 73 (1995) 471.
- [27] B. Lippert (Ed.), *Cisplatin*, Wiley-VCH, Weinheim, 1999.
- [28] (a) M.J. Clarke, V.M. Bailey, P.E. Doan, C.D. Hiller, K.J. LaChance-Galang, H. Daghljan, S. Mandal, C.M. Bastos, D. Lang, *Inorg. Chem.* 35 (1996) 4896;
- (b) I.R. Baird, S.J. Rettig, B.R. James, K.A. Skov, *Can. J. Chem.* 76 (1998) 1379.
- [29] K.B. Reddy, M.-O.P. Cho, J.F. Wishart, T.J. Emge, S.S. Isied, *Inorg. Chem.* 35 (1996) 7241.
- [30] C.A. Tolman, *Chem. Rev.* 77 (1975) 313.
- [31] O. Teichert, W.S. Sheldrick, *Z. Anorg. Allg. Chem.* 625 (1999) 1860.
- [32] R.K.O. Sigel, M. Sabat, E. Freisinger, A. Mower, B. Lippert, *Inorg. Chem.* 38 (1999) 1481.
- [33] C. Singh, *Acta Crystallogr.* 19 (1965) 815.
- [34] E. Ceci, R. Cini, J. Konopa, L. Maresca, G. Natile, *Inorg. Chem.* 35 (1996) 876.
- [35] A.J. Blake, N.R. Champness, R.J. Forder, C.S. Frampton, C.A. Frost, G. Reid, R.H. Simpson, *J. Chem. Soc., Dalton Trans.* (1994) 3377.
- [36] N.J. Holmes, W. Levason, M. Webster, *J. Chem. Soc., Dalton Trans.* (1997) 4223.
- [37] E.R. Brown, J.R. Sandifer, in: B.W. Rossiter, J.F. Hamilton (Eds.), *Physical Methods of Chemistry, Electrochemical Methods*, vol. 2 (chapter 4), Wiley, New York, 1986.
- [38] P.R. Hoffman, K.G. Caulton, *J. Am. Chem. Soc.* 97 (1975) 4221.
- [39] B.R. James, L.R. Markham, *Inorg. Chem.* 13 (1974) 97.
- [40] J.J. Levison, S.D. Robinson, *J. Chem. Soc. A* (1970) 639.
- [41] E.B. McAslan, A.J. Blake, T.A. Stephenson, *Acta Crystallogr.*, C 45 (1989) 1811.
- [42] W.P. Anderson, W.D. Edwards, M.C. Zerner, *Inorg. Chem.* 25 (1986) 2728.
- [43] *HyperChemTM*, Release 5.1 Pro for Windows, Molecular Modeling System, Hypercube Inc., Gainesville, FL, 1997.
- [44] L. Turi, J.J. Dannenberg, *J. Phys. Chem.* 99 (1995) 639.
- [45] S. Scheiner, *Hydrogen Bonding. A Theoretical Perspective*, Oxford University Press, Oxford, 1997.